

## The HI fine structure of HVC 187 near NGC 3783: gas in the leading bridge of the Magellanic System

Bart P. Wakker, Blair D. Savage

*Department of Astronomy, University of Wisconsin, Madison, WI 53706*

Tom A. Oosterloo

*CNR, Istituto di Fisica Cosmica, Milan, Italy*

Mary Putman

*Mount Stromlo and Siding Springs Observatories, Australia*

**Abstract.** We present an analysis of high-resolution HI data of one of the cores of HVC 187 (Wakker & van Woerden 1991), HVC287+22+240. Structure is present down to the lowest-measurable scale ( $\sim 1$  arcmin) and several concentrations appear to be unresolved. Most of the cores seen at low resolution break up into smaller subcores at higher resolution. The typical volume density and pressure are estimated to be  $\sim 30 R^{-1} D_{\text{kpc}}^{-1} \text{ cm}^{-3}$  and  $\sim 18000 R^{-1} D_{\text{kpc}}^{-1} \text{ K cm}^{-3}$ , respectively, where  $R$  is the resolution in arcmin and  $D_{\text{kpc}}$  the unknown distance in kpc.

### 1. Background

Using the Goddard High Resolution Spectrograph (GHRS) on the Hubble Space Telescope (HST), Lu et al. (1998) measured the column density of SII toward HVC 187, using the Seyfert galaxy NGC 3783 as a background probe. This object is one of the main extreme-positive-velocity clouds, defined by Wakker & van Woerden (1991). Using the HI column density derived from the data discussed here, the sulphur abundance was found to be  $0.25 \pm 0.07$  solar, similar to the value in the Magellanic Clouds. Combining this with the tidal model of Gardiner & Noguchi (1996), Lu et al. concluded that the HVC is part of the leading arm of the Magellanic System, implying a distance of 10–50 kpc.

Here we present the HI data used to derive the HI column density. Observations with the Australia Telescope Compact Array (ATCA) were done in June 1994 and March/June 1995, with a resolution of  $60'' \times 38''$ . The primary beam had an FWHM of  $33'.7$ . For calibration, mapping and analysis the MIRIAD software package was used. Cleaning was done using the Multi-Resolution Clean (Wakker & Schwarz 1987). The ATCA data were combined with data from the Parkes Multibeam survey (Staveley-Smith 1997). Figure 1 shows the Parkes map of HVC 187. Other HVCs, with velocities of about  $+100 \text{ km/s}$ , are present in this same region (complex WD).

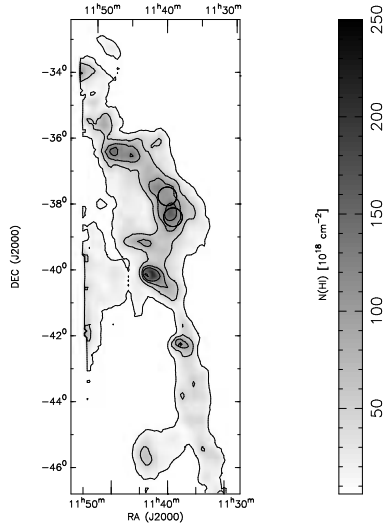


Figure 1. HI column density map of HVC 187 between +204 and +270 km/s, based on Parkes data (16.7 resolution). Contours are at column densities of 10, 50, 90 and  $130 \times 10^{18} \text{ cm}^{-2}$ . The circles near dec.  $-38^\circ$  show the HPBW of the interferometer fields.

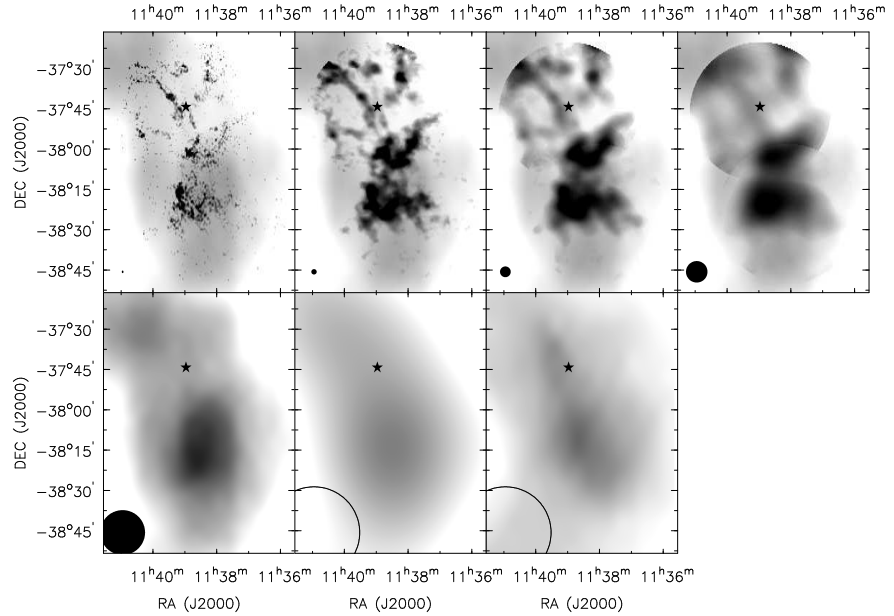


Figure 2. HI column density maps (combined ATCA and Parkes data). Top row, left to right: maps at original  $60'' \times 38''$  resolution, and at  $2' \times 2'$ ,  $4' \times 4'$  and  $8' \times 8'$ . Bottom row, left to right: Parkes map (16.7 beam), Parkes map smoothed to  $34'$ , and Villa Elisa map ( $34'$  beam; Morras & Bajaja 1983). The FWHM sizes of the beams are indicated in the lower left corner of each panel. The black star shows the position of NGC 3783.

## 2. HI maps

Figure 2 shows the total column density map of HVC287+22+240, based on combining ATCA and Parkes data. These maps were created by first summing all interferometer channels, applying a mask. The mask was created by using a 3-sigma cutoff in a map smoothed to double the beam, so that pixels with low S/N ratio could be eliminated. The summed maps were then corrected for primary beam attenuation, converted to brightness temperature, and integrated over velocity. Finally, the two fields were combined. Next, the interferometer and single-dish maps were combined following the method described by Schwarz & Wakker (1991). This consists of smoothing the primary-beam corrected interferometer map to the single-dish beam and subtracting the result from the single-dish map to find the emission that was filtered out by the lack of short interferometer baselines. Adding back the cleaned interferometer map gives the final map.

The resulting map shows the presence of structure at scales of 1 arcmin. Smoothing decreases the apparent column density in the concentrations, indicating that they are not fully resolved. As is usual for high-velocity cloud cores the simple structure seen at  $>20'$  resolution resolves into many scattered cores.

## 3. Spin temperature limits

Figure 3 shows spectra toward the six brightest continuum sources in the field. These spectra were made using the method described by Wakker et al. (1991), using only baselines longer than 180 m. The profiles were extracted, converted to brightness temperature, corrected for primary beam attenuation, and hanning smoothed over 5 points. Table 1 collects the measurements. The spin temperature  $T_s$  follows from the HI emission ( $T_e$ ) and the optical depth of the absorption ( $\tau$ ):  $T_e = T_s(1 - e^{-\tau})$ . We included in  $T_e$  a  $\sim 2$  K contribution from a smooth background (filtered out by the interferometer).

Table 1

#	RA	DEC	Flux	$T_B$	$\tau_{\max}$	S/N	$T_e$	$T_s$
	h m s	d ' "	mJy	K			K	K
(1)	(2)	(3)	(4)	(5)	(6)	(7)	(8)	(9)
1	11 39 34.4	-37 48 37	75.8 $\pm$ 1.4	26.8	0.2	15	<1.6	>19
2	11 39 02.0	-37 44 16	38.7 $\pm$ 1.2	13.7	0.4	8	<2.2	>12
3	11 39 49.2	-37 48 11	45.0 $\pm$ 1.5	15.9	0.4	8	<1.8	>10
4	11 37 34.3	-37 49 55	45.5 $\pm$ 2.7	16.1	0.9	4	=3.8	> 9
5	11 38 59.3	-38 00 47	33.2 $\pm$ 2.1	11.7	1.1	4	=7.4	>14
6	11 40 32.4	-37 40 47	43.1 $\pm$ 2.9	15.2	1.2	4	<3.4	> 8

Col. 1: identification; Col. 2 and 3: position; Cols. 4 and 5: 21-cm continuum flux and corresponding brightness temperature; Col. 6: upper limits to optical depth; Col. 7: S/N ratio of continuum spectrum; Col. 8: peak brightness temperatures or limits on HI emission near the continuum source. Col. 9: lower limits on the spin temperature.

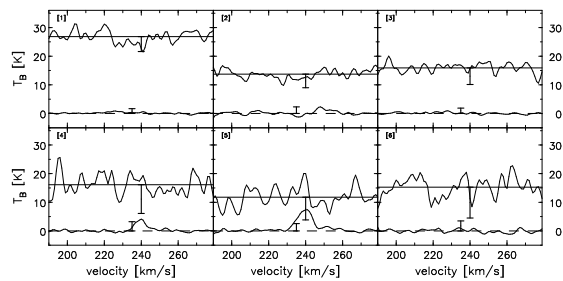


Figure 3. Top lines: emission from the continuum source. Bottom lines: HI emission spectra, found by averaging in a 9x9 pixel box centered on the continuum source, subtracting out the central 5x5 pixels. The vertical bars indicate  $3\sigma$  absorption or emission.

#### 4. Linewidths, densities and pressures

Several concentrations can be discerned (see Figure 2). Figure 4 shows that the brightness temperature decreases with resolution in a manner similar to the expected relation for a  $1'-2'$  gaussian, i.e., they are (almost) unresolved. The run of column density with distance to the center of the blob shows the presence of column density contrasts of a factor 3 on arcminute scales.

Gaussian fits were made to the spectrum at each pixel. Linewidths are 5–10 km/s, increasing slightly with resolution due to beam-smearing of velocity gradients. The components with more extreme velocities tend to occur away from the brightest core at  $11^{\text{h}}39^{\text{m}}, -38^{\circ}15'$ . In low resolution single-dish spectra this would show up as a broadening of the line profiles away from the core. Assuming that the line-of-sight density profile is gaussian, combining the angular diameter ( $\alpha$ ), distance ( $D$ ) and column density ( $N_{\text{H}}$ ) of a concentration yields the volume density:  $n = N_{\text{H}} / (1.064\alpha D)$ . The linewidth,  $W$  (in km/s), is converted to a temperature:  $T = 21.8W^2$ . The pressure then is  $P = nT$ . The derived apparent densities and pressures tend to depend on resolution ( $R$ ), because the measured radius is proportional to  $\sqrt{R}$ , and the column density to  $1/\sqrt{R}$ . The average measured densities of the cores are of the order of  $30 R^{-1} D_{\text{kpc}}^{-1} \text{ cm}^{-3}$ , pressures are  $18000 R^{-1} D_{\text{kpc}}^{-1} \text{ K cm}^{-3}$ . These pressures represent the combined thermal and “turbulent” pressure of the (presumably) cool HI cores.

#### References

- Gardiner L.T., Noguchi M., 1996, MNRAS, 278, 191
- Lu L., Savage B., Sembach K., Wakker B., Oosterloo T., 1998, AJ, 115, 162
- Morras R., Bajaja E., 1983, A&AS, 51, 131
- Schwarz U.J., Wakker B.P., 1991, IAU Coll. 131, p188
- Staveley-Smith L., 1997, PASAu, 14, 111
- Wakker B.P., Vijfschaft B., Schwarz U.J., 1991, A&A, 249, 233
- Wakker B.P., Schwarz U.J., 1987, A&A, 200, 312
- Wakker B.P., van Woerden H., 1991, A&A, 250, 509

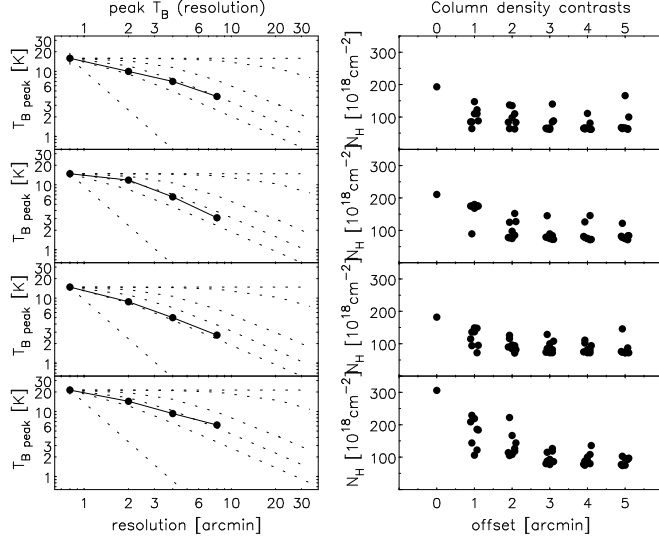


Figure 4. Measurements on concentrations. Left: brightness temperature as function of resolution. Dotted curves give the relations for a point source, a  $1'$ ,  $2'$ ,  $4'$ ,  $20'$  gaussian, and an extended source. Right: run of column density with distance to the center of the concentration.

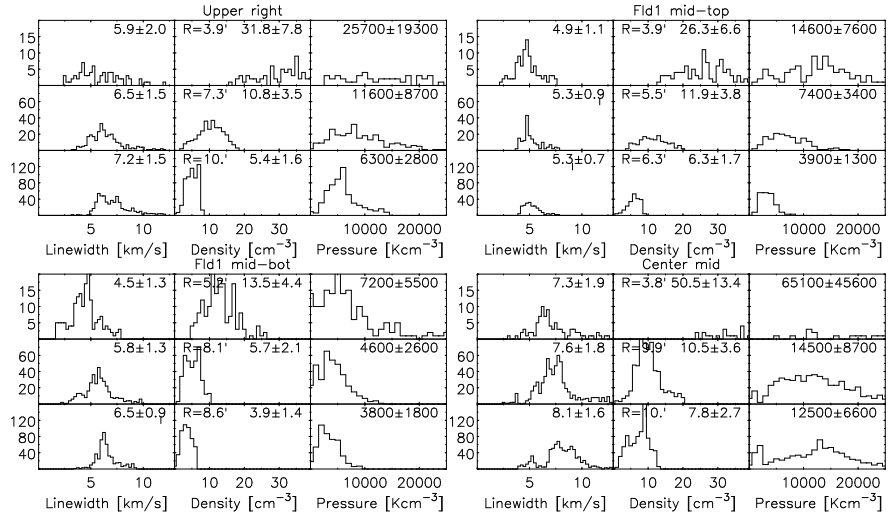


Figure 5. Linewidth, volume density and pressure distribution for all pixels in a concentration for which the column density is  $>0.5$  times the peak value. Nine plots are shown for each concentration, in three rows of three, each row corresponding to  $1'$ ,  $2'$  or  $4'$  resolution.